J. Fluid Mech. (2024), *vol*. 1001, A27, doi:10.1017/jfm.2024.1098

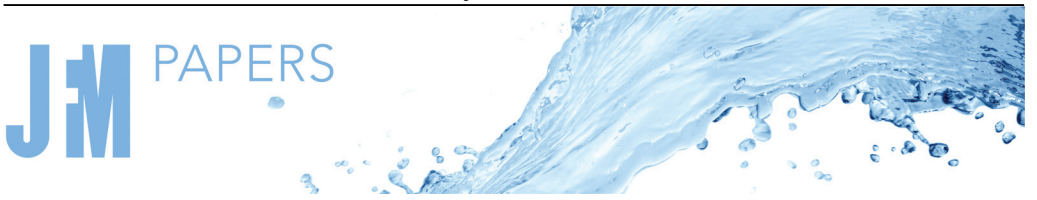

Friction and heat transfer in forced air convection with variable physical properties

Davide Modesti[1],† **and Sergio Pirozzoli**[2]

[1]Gran Sasso Science Institute, Viale Francesco Crispi 7, 67100 L'Aquila, Italy

[2]Dipartimento di Ingegneria Meccanica e Aerospaziale, Sapienza Università di Roma, via Eudossiana 18, 00184 Roma, Italia

(Received 16 April 2024; revised 30 July 2024; accepted 8 November 2024)

We establish a theoretical framework for predicting friction and heat transfer coefficients in variable-property forced air convection. Drawing from concepts in high-speed wall turbulence, which also involves significant temperature, viscosity and density variations, we utilize the mean momentum balance and mean thermal balance equations to develop integral transformations that account for the impact of variable fluid properties. These transformations are then applied inversely to predict the friction and heat transfer coefficients, leveraging the universality of passive scalars transport theory. Our proposed approach is validated using a comprehensive dataset from direct numerical simulations (DNS), covering both heating and cooling conditions up to a friction Reynolds number $Re_\tau \approx 3200$. The predicted friction and heat transfer coefficients closely match the DNS data with accuracy margin 1–2 %, representing a significant improvement over the current state of the art.

Key words: turbulent convection, turbulent boundary layers, compressible turbulence

1. Introduction

Heat transfer by turbulent forced convection occurs when a cold fluid flows over a hot wall, or *vice versa*. Forced thermal convection has countless applications in engineering, and it is the fundamental principle upon which heat exchangers are designed and built (Incropera *et al.* 1996; Kakac, Liu & Pramuanjaroenkij 2002). Heat exchangers are a key component in any energy conversion system – for instance, the radiators in our homes, heat pumps, fuel cells, nuclear plants and solar receivers. In aerospace engineering, two

† Email address for correspondence: davide.modesti@gssi.it

notable applications are aircraft and rocket engines, where components are subjected to extreme heat loads and internal cooling is necessary to guarantee the material integrity.

Most studies on forced thermal convection regard the temperature field as a passive scalar, neglecting its feedback effect on the velocity field through the variation of the transport properties of the fluid. Notable experimental and numerical studies relying on the constant-property assumption are those by Sparrow, Lloyd & Hixon (1966), Xia *et al.* (2022), Alcántara-Ávila, Hoyas & Pérez-Quiles (2021) and Abe & Antonia (2017), together with the more recent direct numerical simulations (DNS) studies performed by our group (Pirozzoli, Bernardini & Orlandi 2016; Pirozzoli & Modesti 2023).

The constant-property assumption is valid if temperature variations are of the order of a few per cent because the thermodynamic variables and fluid properties can be assumed to be constant (Cebeci & Bradshaw 1984). However, most engineering applications feature large temperature differences. For instance, in aircraft engines, the air passing through the cooling channels of turbine blades has mean temperature $T_m \approx 400$ K, whereas the wall temperature reaches $T_w \approx 800$ K, hence their ratio is well beyond the range of validity of the constant-property assumption. This range of temperature variations is common in engineering applications; however, the constant-property assumption is used in most academic research and exploited in engineering practice.

Preliminary design of cooling/heating ducts is based mainly on predictive formulas for the Nusselt number and the pressure drop, which are used for sizing the cooling passages. Among the most classical engineering formulas, we recall those by Dittus & Boelter (1985) and Gnielinski (1976) for the Nusselt number, and Prandtl's friction formula for the pressure drop (Nikuradse 1933). Although their use is widespread in engineering design, these formulas are based on the constant-property assumption and do not directly account for the effect of variable fluid properties, which is usually included using empirical corrections (Sleicher & Rouse 1975; Yeh & Stepka 1984).

The most popular empirical corrections for heat transfer prediction in water are those by Dittus & Boelter (1985) and Sieder & Tate (1936), which account for the fluid viscosity variations through an empirical corrective factor $(\mu_b/\mu_w)^n$ applied to the Nusselt number resulting from formulas obtained for the constant-property case, where μ_m and μ_w are the viscosities of the fluid evaluated at the mean and wall temperatures, respectively. Also for gases, many empirical predictive formulas for the Nusselt number are available, and they have been reviewed extensively by Petukhov (1970) and Yeh & Stepka (1984). However, they all have a structure similar to that used for water, relying on a correction factor based on the mean-to-wall temperature ratio $(T_m/T_w)^n$, with exponent n depending on the type of gas and on the cooling/heating ratio. Similar corrections are also used to estimate the friction factor, and they suggest drag reduction in the case of wall heating, for both liquids (Sieder & Tate 1936) and gases (Yeh & Stepka 1984), compared to the adiabatic case. However, these corrections are fluid-dependent and available for only a limited number of fluids, and their accuracy is often questionable.

More recently, some authors have studied forced thermal convection in fluids with variable properties using DNS. Zonta, Marchioli & Soldati (2012) performed DNS of water flow in a plane channel with a heated wall and a cold wall, and found a reduction of the Reynolds shear stress and of the friction coefficient at the heated wall, despite the lower viscosity, which increases the local Reynolds number. Lee *et al.* (2013) performed DNS of turbulent boundary layers with temperature-dependent viscosity representative of water, and investigated the effect of wall heating on the friction and heat transfer coefficients. They reported a 26 % drag reduction for water with freestream-to-wall temperature ratio

0.77, at freestream temperature approximately 300 K, and the drag reduction mechanism was attributed to a reduction of the wall-shear stress, in agreement with the findings of Zonta *et al.* (2012). Lee *et al.* (2014) used the same DNS dataset to assess heat transfer modifications due to variable viscosity effects, and proposed a correction to the classical Kader fitting for the mean temperature profile (Kader 1981). Patel, Boersma & Pecnik (2016, 2017) studied the effects of variable density and viscosity in liquid-like and gas-like fluids using DNS. They utilized compressibility transformations, originally developed for high-speed boundary layers (Modesti & Pirozzoli 2016; Trettel & Larsson 2016), to map velocity and temperature profiles to the constant-property case, reporting good agreement with the constant-property profiles. Kaller *et al.* (2019) conducted a wall-resolved large-eddy simulation of flow in a duct with one heated side, filled with water, and observed reduced friction near the heated wall, which was also accompanied by weakened secondary flows. The effect of density variations is also important in the context of mixed convection, although the common practice is to rely on the Boussinesq approximation (Pinelli *et al.* 2010; Yerragolam *et al.* 2024), whereas studies that account for a non-Oberbeck–Boussinesq effect are more limited (Zonta 2013). The effect of variable physical properties is also important in pure natural convection (Gray & Giorgini 1976), particularly in experimental studies, where it is challenging to achieve high Rayleigh numbers while satisfying the Oberbeck–Boussinesq approximation. To the best of our knowledge, there is no counterpart of the Grossmann–Lohse theory (Grossmann & Lohse 2000) for Rayleigh–Bénard convection with variable properties.

Although studies focusing on the effect of density and viscosity variations in forced thermal convection are available, predictive formulas for the heat transfer and friction coefficients are invariably based on empirical fitting of experimental data, and the few numerical studies available did not discuss in detail the prediction of these coefficients. In this study, we aim to develop a more solid theoretical framework to estimate the mean friction drag and heat transfer in the presence of variation of the transport properties, focusing on the case of air as the working fluid. For that purpose, we use DNS data of plane turbulent channel flow at a moderate Reynolds number to develop improved formulas for friction and heat transfer prediction.

2. Methodology

We solve the compressible Navier–Stokes equations using our flow solver STREAmS (Bernardini *et al.* 2021, 2023); additional details on the numerical method are reported in Appendix A. The streamwise momentum equation is forced in such a way as to maintain a constant mass flow rate. Periodicity is exploited in the streamwise and spanwise directions, and isothermal no-slip boundary conditions are used at the channel walls. Let h be the half-width of the channel, with DNS carried out in a computational domain $L_x \times L_y \times L_z = 6\pi h \times 2h \times 2\pi h$. A uniform bulk cooling or heating term is added to the entropy equation to guarantee that the mixed mean temperature, defined as

$$T_m = \frac{1}{2h\rho_b u_b}\int_0^{2h} \bar{\rho}\,\bar{u}\,\bar{T}\,\mathrm{d}y, \quad \rho_b = \frac{1}{2h}\int_0^{2h} \bar{\rho}\,\mathrm{d}y, \quad u_b = \frac{1}{2h\rho_b}\int_0^{2h} \bar{\rho}\,\bar{u}\,\mathrm{d}y, \quad (2.1a\text{–}c)$$

remains exactly constant in time. Here, ρ_b and u_b are the bulk density and velocity, respectively. In the following, an overline is used to indicate Reynolds averaging in time and in the homogeneous spatial directions, and a prime is used to denote fluctuations thereof. As is common in variable-density flows, we also use Favre averages, denoted with a tilde as $\tilde{f} = \overline{\rho f}/\bar{\rho}$, and a double prime will indicate fluctuations thereof.

A + superscript is used to denote normalization by wall units, namely by friction velocity $u_\tau = (\tau_w/\bar{\rho}_w)^{1/2}$ (where $\tau_w = \mu_w \, \mathrm{d}\tilde{u}/\mathrm{d}y|_w$ is the mean wall shear stress), and the associated viscous length scale $\delta_v = \nu_w/u_\tau$, where the subscript w denotes quantities evaluated at the wall. For inner normalization of the mean temperature, we use the friction temperature $\theta_\tau = q_w/(\rho_w c_p u_\tau)$, where $q_w = \lambda_w \, \mathrm{d}\tilde{T}/\mathrm{d}y|_w$ is the mean wall heat flux, $c_p = \gamma/(\gamma - 1)R$ is the specific heat capacity at constant pressure, R is the air constant, and λ_w is the thermal conductivity at the wall, evaluated as $\lambda = \mu c_p/Pr$, with Prandtl number set to $Pr = 0.72$.

Twenty DNS have been carried out at bulk Mach number $M_b = u_b/c_m = 0.2$ (where c_m is the speed of sound at the mixed mean temperature) and bulk Reynolds number $Re_b = 2\rho_b u_b h/\mu_m \approx 9000$–$70\,000$ (see table 1), where $\mu_m = \mu(T_m)$ is the dynamic viscosity evaluated at the mixed mean temperature, as obtained from Sutherland's law (White 1974). The Mach number is low enough that compressibility effects are negligible, as it turns out, in order to isolate variable-property effects. We consider various mean-to-wall temperature ratios, namely $T_m/T_w = 0.4, 0.5, 0.7, 0.8, 1.5, 2, 2.5, 3$, resulting in friction Reynolds numbers in the range $Re_\tau = u_\tau h/\nu_w \approx 150$–$3200$, where ν_w is the kinematic viscosity at the wall. For the case of mean-to-wall temperature ratio $T_m/T_w = 0.5$, we also study the effect of varying the dimensional wall temperature, considering cases with $T_w = 800$ and 293.15 K. This temperature range is rather wide and covers most applications of forced air convection of which we are aware. Cases with wall heating approach the condensation temperature of air ($\approx$90 K), and cases with wall cooling feature temperature variations in the range 220 K $\lesssim T \lesssim$ 1000 K, involving temperature values beyond those normally found in heat exchangers. For each value of the mean-to-wall temperature ratio, we have two flow cases, denoted with the letters L and H, depending on whether the Reynolds number is comparatively 'low' or 'high' (see table 1). For two flow cases with mean-to-wall temperature ratio $T_m/T_w = 0.5$ and $T_m/T_w = 2$ we also consider a 'very high' Reynolds number case, denoted with VH. In the present study, we consider pure forced convection, neglecting the effect of buoyancy because in forced air convection applications the Richardson number is typically very small. For instance, cooling channels of turbine blades have bulk velocity $u_b \approx 30$–60 m s^{-1} and temperature variations of order 400 K, leading to Richardson numbers of the order $Ri \approx 10^{-5}$.

3. Instantaneous temperature field

We begin our analysis by inspecting the instantaneous velocity and temperature fields of flow cases H05-A (wall heating) and H3 (wall cooling) in figure 1. Both cases exhibit the qualitative features that characterize wall turbulence, with high-speed cold (or hot) flow structures protruding towards the walls, and low-speed hot (or cold) fluid regions protruding towards the channel centre. Despite sharing the general features of wall turbulence, we also note a significant effect of the thermodynamic and fluid property variations between cases with wall heating and wall cooling. First, we observe that the friction Reynolds number values reported in table 1 are not indicative of actual separation of scales in constant-property flows. For instance, flow case with wall heating H05-A ($T_m/T_w = 0.5$) has a relatively low friction Reynolds number ($Re_\tau = 360$), but it exhibits finer eddies than one would expect at this Reynolds number. This effect can be traced to strong viscosity variations within the near-wall and core flow regions. The opposite is true for wall cooling; for instance, flow case H3 ($T_m/T_w = 3$) has a higher friction Reynolds number ($Re_\tau = 1420$), but small scales are absent and the flow appears to be a

https://doi.org/10.1017/jfm.2024.1098 Published online by Cambridge University Press

	Re_b	Re_τ	T_m/T_w	T_w (K)	$Re_{\tau,cp}$	$C_f \times 10^3$	$St \times 10^3$	Nu	N_x	N_y	N_z	Δx^*	Δy_w^*–Δy_{max}^*	Δz^*
L04	17 182	155	0.4	800	533	5.45	3.09	38.3	1024	280	512	9.8	0.69–5.1	6.5
L05-A	20 170	212	0.5	293.15	612	5.57	3.18	46.2	1024	280	512	11.3	0.67–5.9	7.5
L05-B	17 115	205	0.5	800	511	5.62	3.21	39.5	1024	280	512	9.4	0.58–4.9	6.3
L07	13 565	255	0.7	800	400	6.28	3.56	34.8	1024	280	512	7.4	0.40–3.8	4.9
L08	16 679	356	0.8	800	470	6.01	3.4	40.9	1024	280	512	8.7	0.47–4.5	5.8
L15	14 632	663	1.5	800	406	6.82	4.1	43.2	1024	280	512	7.5	0.41–3.9	5
L2	11 389	789	2	293.15	317	7.31	4.37	35.9	1024	280	512	5.8	0.32–3.0	3.9
L25	9853	902	2.5	293.15	278	7.75	4.62	32.8	1024	280	512	5.1	0.28–2.7	3.4
L3	9212	1051	3	293.15	261	8.04	4.78	31.7	1024	280	512	4.8	0.18–2.5	3.2
H04	31 797	260	0.4	800	893	4.52	2.59	59.3	2048	480	1024	8.2	0.66–5.0	5.5
H07	37 887	617	0.7	800	971	4.75	2.73	74.5	2048	480	1024	8.9	0.45–5.4	6
H05-A	37 589	360	0.5	293.15	1040	4.66	2.68	72.5	2048	480	1024	9.6	0.37–5.8	6.4
H05-B	37 933	404	0.5	800	1007	4.47	2.57	70.3	2048	480	1024	9.3	0.57–5.6	6.2
H08	34 703	674	0.8	800	890	4.97	2.83	70.7	2048	480	1024	8.2	0.41–5.0	5.5
H15	18 694	861	1.5	293.15	498	6.3	3.78	50.8	2048	480	1024	4.6	0.27–2.8	3.1
H2	15 362	1028	2	293.15	415	6.81	4.06	44.9	2048	480	1024	3.8	0.15–2.3	2.5
H25	13 873	1224	2.5	293.15	378	7.15	4.26	42.5	2048	480	1024	3.5	0.13–2.1	2.3
H3	12 898	1420	3	293.15	354	7.44	4.42	41.1	2048	480	1024	3.3	0.12–2.0	2.2
VH05	68 874	680	0.5	800	1687	3.85	2.22	110.3	4096	800	2048	7.8	0.30–5.6	5.2
VH2	54 439	3201	2	293.15	1298	5.22	3.13	122.9	4096	800	2048	6	0.23–4.3	4

Table 1. Flow parameters for plane channel flow DNS. Box dimensions are $6\pi h \times 2h \times 2\pi h$ for all flow cases; $Re_b = 2\rho_b h u_b/\nu_m$ is the bulk Reynolds number, and $Re_\tau = h u_\tau/\nu_w$ is the friction Reynolds number; $Re_{\tau,cp} = y_{cp}(h)/\delta_v$ is the equivalent friction Reynolds number, defined in equation; T_m and T_w are the mixed mean temperature and the wall temperature, respectively; $C_f = 2\tau_w/(\rho_b u_b^2)$ is the friction coefficient; $St = q_w/[\rho_b C_p u_b (T_w - T_m)]$ is the Stanton number; $Nu = St\, Re_b\, Pr$ is the Nusselt number; Δx and Δz are the mesh spacings in the streamwise and spanwise directions, and Δy_w is the mesh spacing at the wall; and the $*$ superscript indicates normalization with equivalent constant-property viscous length scale $\delta_{v,cp}$, defined in (4.16*c*).

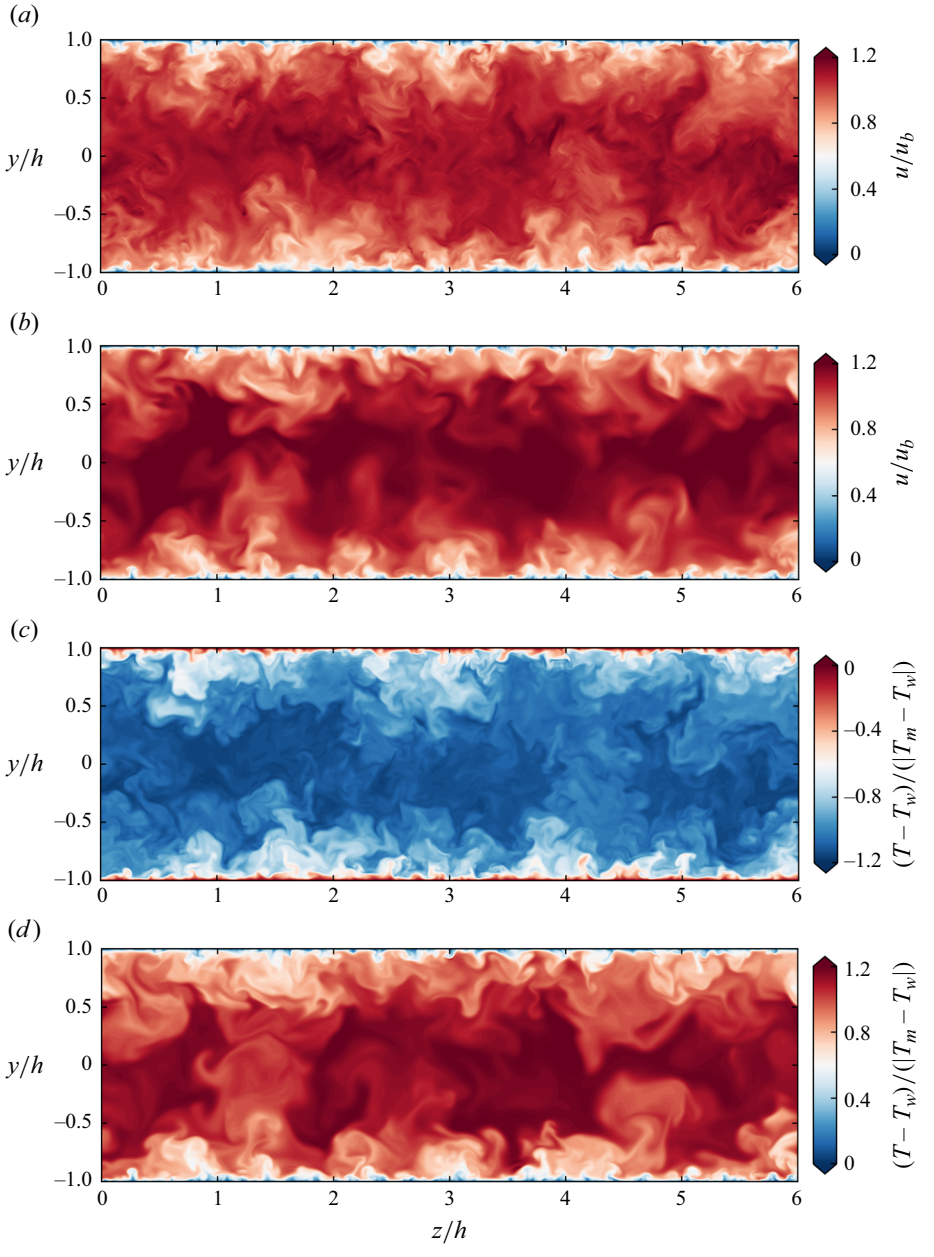

Figure 1. Instantaneous (a,b) velocity and (c,d) temperature fields in a cross-stream plane, for flow cases (a,c) H05-A (wall heating, $Re_\tau = 360$, $T_m/T_w = 0.5$) and (b,d) H3 (wall cooling, $Re_\tau = 1420$, $T_m/T_w = 3$).

'low-pass filtered' version of the heated case, in which only large structures survive. In fact, in flow case H3 we observe large structures extending from one wall to beyond the channel centreline, whereas those are masked by smaller eddies in flow case H05-A.

We note that the instantaneous velocity and temperature fields are highly correlated, which is to be expected due to the similarity of the underlying equations and the near-unity value of the Prandtl number, hence the Reynolds analogy holds qualitatively also for the case of variable fluid properties. Close scrutiny of the kinematic and thermal fields reveals

that temperature has finer structures as compared to velocity, which is due partly to the Prandtl number being lower than unity, and partly to the effect of the pressure gradient term in the momentum equation (A1*b*), which is absent in the energy equation (A1*c*) (Pirozzoli *et al.* 2016). The occurrence of sharper eddy boundaries in passive scalars compared to the velocity field, even at unit Prandtl number, is a well-known feature that has been reported by several authors (Kim, Guezennec & Stretch 1990; Abe & Antonia 2017), and it has been associated with the unmixedness of the scalar, as the absence of the pressure gradient results in reduced heat transport as compared to momentum transport.

4. Mean flow field and variable-property transformations

We begin the mean flow analysis by comparing the mean velocity and temperature profiles to the equivalent statistics for the constant-property case. For that purpose, we rely both on DNS data of constant-property plane channel flow with passive scalar transport at $Pr = 0.71$ from Pirozzoli *et al.* (2016), and on synthetic composite profiles, which are obtained by matching inner-layer velocity and temperature profiles with the corresponding outer-layer distributions. The inner-layer profiles are obtained by integrating the eddy viscosity of Musker (1979) for the velocity, and the eddy diffusivity proposed by Pirozzoli (2023) for the temperature profile. In the outer layer, we use Clauser's hypothesis of uniform eddy viscosity (Clauser & Francis 1956) and uniform eddy diffusivity (Pirozzoli *et al.* 2016). A complete derivation of the composite profiles is available in Pirozzoli & Modesti (2024). Figure 2 shows that the composite profiles of mean temperature and velocity for the constant-property case are essentially indistinguishable from the DNS data, with the advantage that the synthetic profiles are available at any Reynolds number and Prandtl number.

We note that the statistics of the variable-property DNS are substantially different from those in the constant-property case when scaled in classical wall units. All the flow cases exhibit deviations from the reference, starting from the buffer region, and becoming more evident in the logarithmic region, where both the logarithmic slope and the additive constant deviate from the constant-property references. Hence we conclude that in the variable-property case, the law-of-the-wall for both the mean velocity and temperature is not universal, but rather depends on the specific mean-to-wall temperature ratio.

In analogy with what is done for compressible flows, we assume that the effects of density and viscosity variations can be accounted for using suitable convolution integrals (Modesti & Pirozzoli 2016)

$$y_{cp} = \int_0^y f_{cp}\,\mathrm{d}y, \quad u_{cp} = \int_0^{\tilde{u}} g_{cp}\,\mathrm{d}\tilde{u}, \quad \theta_{cp} = \int_0^{\tilde{\theta}} h_{cp}\,\mathrm{d}\tilde{\theta}, \tag{4.1a–c}$$

with kernel functions f_{cp}, g_{cp}, h_{cp} to be specified such that the flow properties are mapped to the universal, constant-property case, denoted with the 'cp' subscript. In order to account for the variable-property effect, we consider the streamwise mean momentum balance equation

$$\overline{\mu' \frac{\mathrm{d}u'}{\mathrm{d}y}} + \bar{\mu}\frac{\mathrm{d}\tilde{u}}{\mathrm{d}y} - \bar{\rho}\,\widetilde{u''v''} = \bar{\rho}_w u_\tau^2 (1-\eta), \tag{4.2}$$

where $\eta = y/h$. Following Hasan *et al.* (2023), we then introduce an eddy viscosity for the turbulent shear stress, such that $-\bar{\rho}\,\widetilde{u''v''} = \bar{\rho}\nu_T\,\mathrm{d}\tilde{u}/\mathrm{d}y$. Substituting the transformations

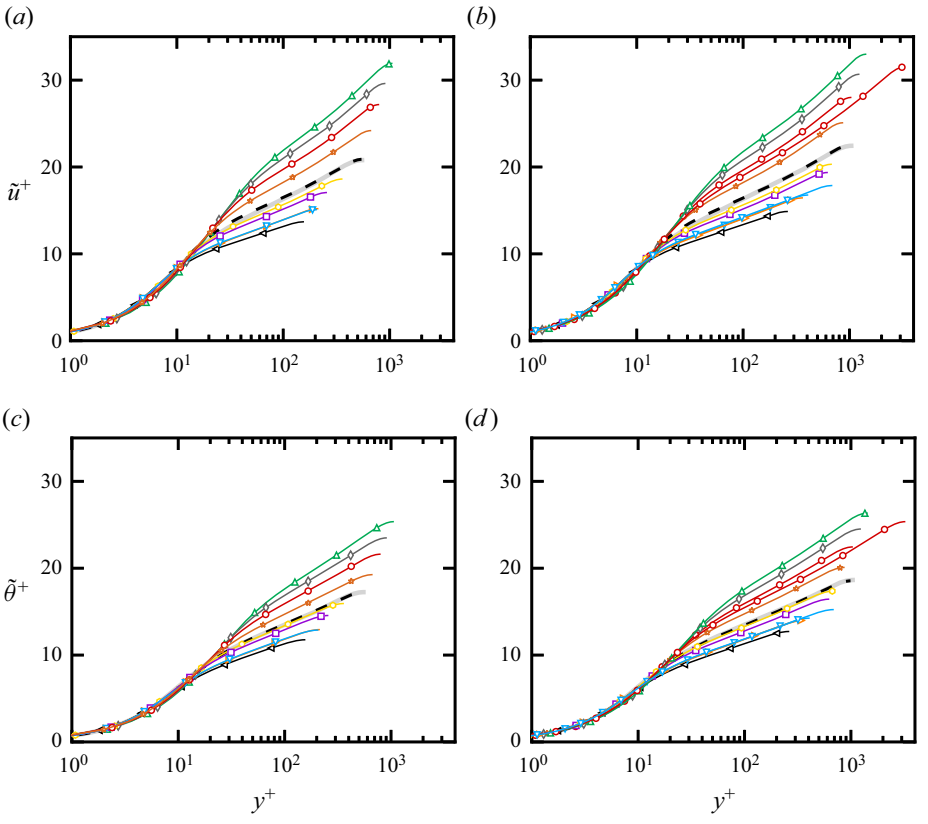

Figure 2. (*a*,*b*) Mean velocity and (*c*,*d*) mean temperature profiles for (*a*,*c*) L flow cases and (*b*,*d*) H flow cases. Symbols indicate DNS data for different mean-to-wall temperature ratios: $T_m/T_w = 0.4$ (left triangles), $T_m/T_w = 0.5$, $T_w = 800$ K (downward triangles), $T_m/T_w = 0.5$, $T_w = 273.25$ K (right triangles), $T_m/T_w = 0.7$ (squares), $T_m/T_w = 0.8$ (hexagons), $T_m/T_w = 1.5$ (stars), $T_m/T_w = 2$ (circles), $T_m/T_w = 2.5$ (diamonds), $T_m/T_w = 3$ (upward triangles). The grey solid lines indicate the mean velocity and temperature profiles of the constant-property case at $Pr = 0.72$, obtained using the composite profiles of Pirozzoli & Modesti (2024). The dashed black lines indicate DNS of constant-property channel flow from Pirozzoli *et al.* (2016) at $Pr = 0.71$.

(4.1*a*–*c*) into the streamwise mean momentum balance equation, and assuming $\overline{\mu' \, \mathrm{d}u'/\mathrm{d}y} \approx 0$, one obtains

$$\frac{\bar{\mu}}{\mu_w}\frac{f_{cp}}{g_{cp}}\left(1+\frac{\nu_T}{\nu}\right)\frac{\mathrm{d}u^+_{cp}}{\mathrm{d}y^+_{cp}} = 1-\eta. \tag{4.3}$$

Comparing (4.3) with the constant-property counterpart

$$\left(1+\frac{\nu_{T,cp}}{\nu_{cp}}\right)\frac{\mathrm{d}u^+_{cp}}{\mathrm{d}y^+_{cp}} = 1-\eta, \tag{4.4}$$

we find the following relation between the two kernel functions f_{cp} and g_{cp}:

$$\frac{\bar{\mu}}{\mu_w}\frac{f_{cp}}{g_{cp}}\left(1+\frac{\nu_T}{\nu}\right) = 1+\frac{\nu_{T,cp}}{\nu_{cp}}. \tag{4.5}$$

A second condition is needed, which we find by enforcing that van Driest scaling (van Driest 1951) holds in the logarithmic region, as done by Trettel & Larsson (2016).

With this condition, we find

$$f_{cp} = \frac{\mathrm{d}}{\mathrm{d}y}\left(\frac{y}{R^{1/2}N}\right), \quad g_{cp} = \left(\frac{1+\nu_T/\nu}{1+\nu_{T,cp}/\nu}\right) RN \frac{\mathrm{d}}{\mathrm{d}y}\left(\frac{y}{R^{1/2}N}\right), \tag{4.6a,b}$$

where $N = \bar{\nu}/\nu_w$ and $R = \bar{\rho}/\bar{\rho}_w$. The kernel functions (4.6*a*,*b*) are formally equivalent to the velocity transformation derived by Hasan *et al.* (2023) for a high-speed turbulent boundary layer, with eddy viscosities to be specified. Using the model eddy viscosity of Musker (1979) for the baseline case of constant-property flow, herein we extend the model to account for variable-property effects by including an *ad hoc* correction depending on the mean-to-wall temperature ratio

$$\frac{\nu_{T,cp}}{\nu} = \frac{(\kappa y^+_{cp})^3}{(\kappa y^+_{cp})^2 + C^2_{v1}}, \quad \frac{\nu_T}{\nu} = \frac{(\kappa y^+_{cp})^3}{(\kappa y^+_{cp})^2 + C^2_{v1} + \varphi(T_m/T_w)}, \tag{4.7a,b}$$

where $\kappa = 0.387$ is the assumed Kármán constant, and $C_{v1} = 7.3$. Fitting the present DNS data (only flow cases at 'high Reynolds numbers', denoted as H, have been taken into account), we have determined empirically the following expressions for the additive function φ:

$$\varphi(T_m/T_w) = \begin{cases} -32\log(T_m/T_w) - 59(1-T_m/T_w)^2, & T_m/T_w < 1, \\ 5.6(1-T_m/T_w), & T_m/T_w > 1. \end{cases} \tag{4.8}$$

Similarly to what is done for the mean velocity, a transformation for the mean temperature profile is obtained starting from the mean energy balance equation

$$\underbrace{\overline{\lambda' \frac{\mathrm{d}\theta'}{\mathrm{d}y}}}_{\textit{fluctuating conduction}} + \underbrace{\bar{\lambda}\frac{\mathrm{d}\tilde{\theta}}{\mathrm{d}y}}_{\textit{mean conduction}} \underbrace{- C_p\bar{\rho}\,\widetilde{\theta''v''}}_{\textit{turbulent convection}} + \underbrace{\Psi}_{\textit{dissipation}} = \underbrace{q_w(1-\mathcal{R})}_{\textit{total heat flux}}, \tag{4.9}$$

where

$$\mathcal{R}(\eta) = \frac{1}{\rho_b}\int_0^\eta \bar{\rho}(\eta)\,\mathrm{d}\eta, \quad \Psi = \int_0^y \epsilon\,\mathrm{d}y - \int_0^y \frac{\rho}{\rho_b}\int_0^1 \epsilon\,\mathrm{d}\eta\,\mathrm{d}y, \tag{4.10a,b}$$

$$\epsilon = \overline{\sigma_{ij}\frac{\partial u_i}{\partial x_j}} - \overline{u_i\frac{\partial p}{\partial x_i}}. \tag{4.10c}$$

The relative importance of the different terms in (4.6) is analysed in figure 3, for representative flow cases with wall heating and wall cooling. Figure 3 shows that the mean temperature balance of variable-property flows is qualitatively similar to what is found in passive scalar convection, with mean conduction dominating the near-wall region, and turbulent convection dominating the overall balance away from the wall. However, notable differences are the nonlinearity of the total heat flux (on account of the definition of $\mathcal{R}$) and the presence of additional terms that are small but not zero. Indeed, very close to the wall, we find a small contribution from the fluctuating conduction term, which, however, remains much smaller than the mean conduction. We recall that in the mean momentum equation (4.2) the fluctuating diffusion term $\overline{\mu'\,\mathrm{d}u'/\mathrm{d}y}$ was neglected, which yields a similar contribution to momentum balance as $\overline{\lambda'\,\mathrm{d}T'/\mathrm{d}y}$ yields to the temperature balance (not shown). The dissipation remains negligible for all cases considered here,

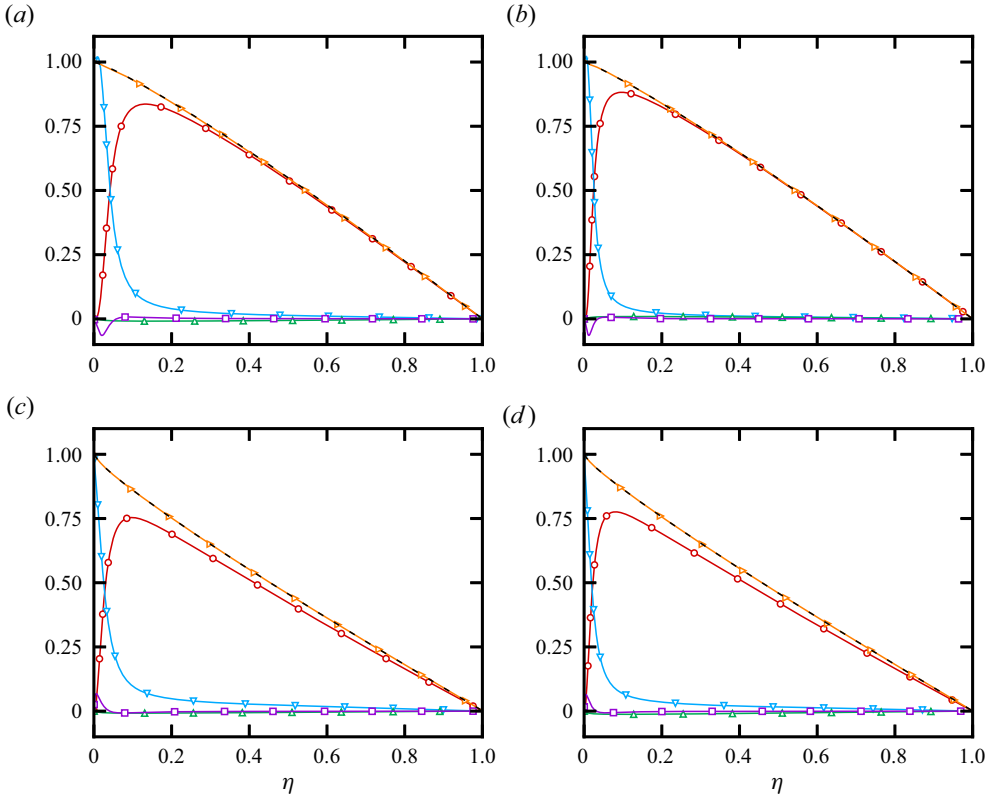

Figure 3. Mean energy balance as in (4.9) for flow cases (*a*) L05-A ($Re_\tau = 212$, $T_m/T_w = 0.5$), (*b*) H05-A ($Re_\tau = 360$, $T_m/T_w = 0.5$), (*c*) L3 ($Re_\tau = 1051$, $T_m/T_w = 3$), and (*d*) H3 ($Re_\tau = 1420$, $T_m/T_w = 3$). The symbols indicate mean conduction (downward triangles), fluctuating conduction (squares), turbulent convection (circles), dissipation (upward triangles), total heat flux $\mathcal{R}(\eta)$ in (4.9) (dashed black line), and sum of the different contributions (right triangles).

due to the small Mach number under scrutiny, confirming that all flow cases can be regarded as representative of incompressible flow. We also note that the total stress $\mathcal{R}(\eta)$ in (4.10) is indistinguishable from the sum of the components, indicating excellent statistical convergence of the results.

Based on the DNS data, we then assume $\Psi \approx 0$ and $\overline{\lambda' \,\mathrm{d}\theta'/\mathrm{d}y} \approx 0$, and in analogy with what is done for the turbulent shear stress, we model the turbulent heat flux by introducing a thermal eddy diffusivity, such that

$$\widetilde{\theta'' v''} \, \frac{1-\eta}{1-\mathcal{R}} = -\alpha_T \, \frac{\mathrm{d}\tilde{\theta}}{\mathrm{d}y}. \tag{4.11}$$

Following the same procedure as used for the mean momentum equation, we then determine the corresponding kernel function

$$h_{cp} = \left(\frac{1+\alpha_T/\alpha}{1+\alpha_{T,cp}/\alpha} \right) \frac{1-\eta}{1-\mathcal{R}} \, RN \, \frac{\mathrm{d}}{\mathrm{d}y} \left(\frac{y}{R^{1/2} N} \right), \tag{4.12}$$

where $\alpha = \lambda/(\rho c_p)$ is the thermal diffusivity coefficient. Following Pirozzoli (2023), we model the turbulent diffusivity as

$$\frac{\alpha_{T,cp}}{\alpha} = \frac{(\kappa_\theta y^+_{cp})^3}{(\kappa_\theta y^+_{cp})^2 + C^2_{v3}}, \quad \frac{\alpha_T}{\alpha} = \frac{(\kappa_\theta y^+_{cp})^3}{(\kappa_\theta y^+_{cp})^2 + C^2_{v3} + \beta(T_m/T_w)}, \tag{4.13a,b}$$

with constants $\kappa_\theta = 0.459$, $C_{v3} = 10$. As for the mean velocity, the dependency of the eddy thermal diffusivity on mean-to-wall temperature ratio is accounted for empirically by fitting the DNS data, to obtain

$$\beta(T_m/T_w) = \begin{cases} (1 - T_m/T_w)[141 - 507(T_m/T_w) + 608(T_m/T_w)^2], & T_m/T_w < 1, \\ -28\log(T_m/T_w) + 1.6(1 - T_m/T_w)^2, & T_m/T_w > 1. \end{cases} \tag{4.14}$$

To summarize, the kernel functions (4.6*a*,*b*) and (4.12) are rooted in the mean momentum balance and temperature balance equations, with eddy viscosity and eddy conductivity to be specified. This is, in our opinion, more robust that relying entirely on data-driven transformations (Volpiani *et al.* 2020). Nonetheless, we are not aware of any exact result in turbulence theory that does not include constants to be determined from experience or simulation, and the present case is no exception. Here, the constants κ, κ_θ, C_{v1} and C_{v3} were determined once and for all for constant-property flow (Pirozzoli *et al.* 2021; Pirozzoli & Modesti 2023). The only added ingredients here are the functions φ in (4.8) and β in (4.14), which account empirically for the dependency on the bulk-to-wall temperature ratio. We note that both (4.8) and (4.14) show different functional dependency for heating and cooling, which is aligned with empirical formulas for the Nusselt number and friction coefficient reported in the literature (Petukhov 1970; Yeh & Stepka 1984), featuring different coefficients or functions for the two cases.

In figure 4, we plot the transformed mean velocity and temperature profiles using the kernel functions (4.6*a*,*b*) and (4.13*a*,*b*), and compare the results with the reference constant-property case. The universality of the various distributions is quite remarkable, given the wide range of variation of the flow properties that we are considering. The accuracy of the velocity and temperature transformations also supports the validity of the assumptions made to derive the kernel functions for the convolution integrals (4.1*a*–*c*). We point out that the coefficients inferred from DNS have been calibrated only for flow cases H, and they are successfully applied to lower or higher Reynolds numbers with similar accuracy, showing substantial independence from the Reynolds number. These transformations allow us to define an equivalent channel height h_{cp}, which we use to introduce an equivalent constant-property friction Reynolds number,

$$Re_{\tau,cp} = \frac{h_{cp}}{\delta_v}, \quad h_{cp} = \int_0^h f_{cp}\,\mathrm{d}y. \tag{4.15a,b}$$

The equivalent channel height h_{cp} is larger than h for heating, and smaller for cooling, leading to higher or lower equivalent constant-property friction Reynolds numbers, respectively. The definition given in (4.15*a*,*b*) can also be used to define an equivalent constant-property friction velocity, and an equivalent viscous length scale, namely

$$Re_{\tau,cp} = \frac{u_{\tau,cp} h}{\bar{\nu}_w}, \quad u_{\tau,cp} = \frac{\bar{\nu}_w}{\delta_{v,cp}}, \quad \delta_{v,cp} = \frac{h}{h_{cp}}\,\delta_v. \tag{4.16a–c}$$

Values of the equivalent constant-property Reynolds numbers are reported in table 1, which can be used as a guide to interpret the instantaneous flow field in figure 1, where

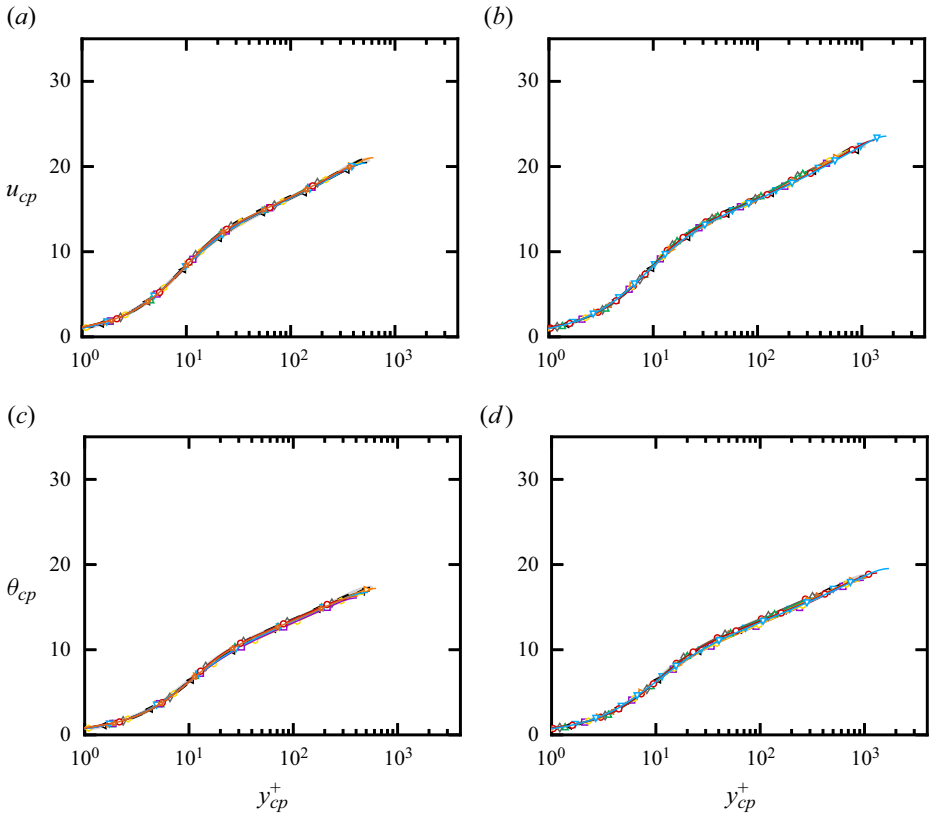

Figure 4. (*a*,*b*) Mean velocity and (*c*,*d*) mean temperature profiles transformed using (4.1*a–c*) with kernel functions (4.6*a*,*b*) and (4.13*a*,*b*), for (*a*,*c*) L flow cases and (*b*,*d*) H flow cases. Symbols indicate DNS data for different mean-to-wall temperature ratios: $T_m/T_w = 0.4$ (left triangles), $T_m/T_w = 0.5$, $T_w = 800$ K (downward triangles), $T_m/T_w = 0.5$, $T_w = 273.25$ K (right triangles), $T_m/T_w = 0.7$ (squares), $T_m/T_w = 0.8$ (hexagons), $T_m/T_w = 1.5$ (stars), $T_m/T_w = 2$ (circles), $T_m/T_w = 2.5$ (diamonds), $T_m/T_w = 3$ (upward triangles). The grey solid lines indicate the reference mean velocity and temperature profiles of the constant-property case at $Pr = 0.72$, obtained using the synthetic velocity profile of Musker (1979) and the synthetic temperature profile of Pirozzoli (2023). The dashed black lines indicate DNS of constant-property channel flow from Pirozzoli *et al.* (2016) at $Pr = 0.71$.

flow cases with heating show finer eddies than for cooling because their effective Reynolds number is higher.

5. Wall friction and heat transfer

The variable-property transformations developed in the previous section are very useful, especially as they enable the prediction of the heat transfer and friction coefficients. For that purpose, the only required inputs are the reference constant-property mean velocity and mean temperature profiles. As discussed previously, in the current work we consider the composite profiles developed in the work of Pirozzoli & Modesti (2024). However, different choices are possible, and one could, for instance, use the model for the mean velocity by Nagib & Chauhan (2008), and the model for the mean temperature by Kader (1981), although the latter might result in less accurate temperature profiles

Algorithm 1 Inverse variable-property transformation, where ε_{Re_τ} and ε are the tolerances for the iterative algorithm, which in our case are set to 10^{-9} and 10^{-10}, respectively.

Initialization:

Generate constant-property profiles for a prescribed target value of $Re_{\tau,cp}$: u^n_{cp}, θ^n_{cp}

Set:$u^n = u^n_{cp}$, $\theta^n = \theta^n_{cp}$, Calculate: f^n_{cp}, g^n_{cp}, h^n_{cp}, C^n_f, St^n using θ^n for a given T_m/T_w

while $(|Re^n_{\tau,cp} - Re_{\tau,cp}| < \varepsilon_{Re_\tau})$ **do**

while $(|C^{n+1}_f - C^n_f| < \varepsilon)$ and $(|St^{n+1} - St^n| < \varepsilon)$ **do**

$$y^{n+1} = \int \frac{1}{f^n_{cp}}\,\mathrm{d}y^n_{cp}, \quad \tilde{u}^{n+1} = \int \frac{1}{g^n_{cp}}\,\mathrm{d}u^n_{cp}, \quad \tilde{\theta}^{n+1} = \int \frac{1}{h^n_{cp}}\,\mathrm{d}\theta^n_{cp}$$

Update kernels: f^{n+1}_{cp}, g^{n+1}_{cp}, h^{n+1}_{cp}, using (4.6*a*,*b*)–(4.12)

Update coefficients and Reynolds number: C^{n+1}_f, St^{n+1}, $Re^{n+1}_{\tau,cp}$ using (4.15*a*,*b*)

Update constant-property profiles u^{n+1}_{cp}, θ^{n+1}_{cp} at $Re^{n+1}_{\tau,cp}$

end while

end while

due to inconsistencies in the near-wall region. Starting from those, application of the inverses of transformations (4.1*a–c*),

$$y = \int_0^y \frac{1}{f_{cp}}\,\mathrm{d}y_{cp}, \quad \tilde{u} = \int_0^{u_{cp}} \frac{1}{g_{cp}}\,\mathrm{d}u_{cp}, \quad \tilde{\theta} = \int_0^{\theta_{cp}} \frac{1}{h_{cp}}\,\mathrm{d}\theta_{cp}, \tag{5.1a–c}$$

allows us to determine the actual variable-property profiles, for any given mean-to-wall temperature ratio and Reynolds number. The key technical difficulty is that the kernel functions f_{cp}, g_{cp}, h_{cp} depend on the actual temperature in the variable-property case, hence an iterative procedure is necessary, as for compressible flow (Kumar & Larsson 2022; Hasan *et al.* 2024). The iterative procedure is presented in Algorithm 1, and it can be summarized as follows.

(i) Generate the constant-property profiles for a target friction Reynolds number $Re_{\tau,cp}$.
(ii) Initialize kernel functions f_{cp}, g_{cp}, h_{cp} using the constant-property temperature profile.
(iii) Calculate the backward convolution integrals (5.1*a–c*) to find y, u, θ.
(iv) Update the kernels f_{cp}, g_{cp}, h_{cp} using the newly calculated temperature θ.
(v) Calculate the friction coefficient, the Stanton number and $Re_{\tau,cp}$.
(vi) Update the constant-property profiles based on the updated $Re_{\tau,cp}$.

Note that two nested loops are required for this iterative algorithm. This is because the constant-property profiles are also recalculated at each step in order to converge towards the target friction Reynolds number $Re_{\tau,cp}$.

Figure 5 shows the resulting friction coefficient $C_f = 2\tau_w/(\rho_b u_b^2)$ and the Stanton number $St = q_w/[\rho_b C_p u_b (T_w - T_m)]$. Whereas the data for the constant-property case

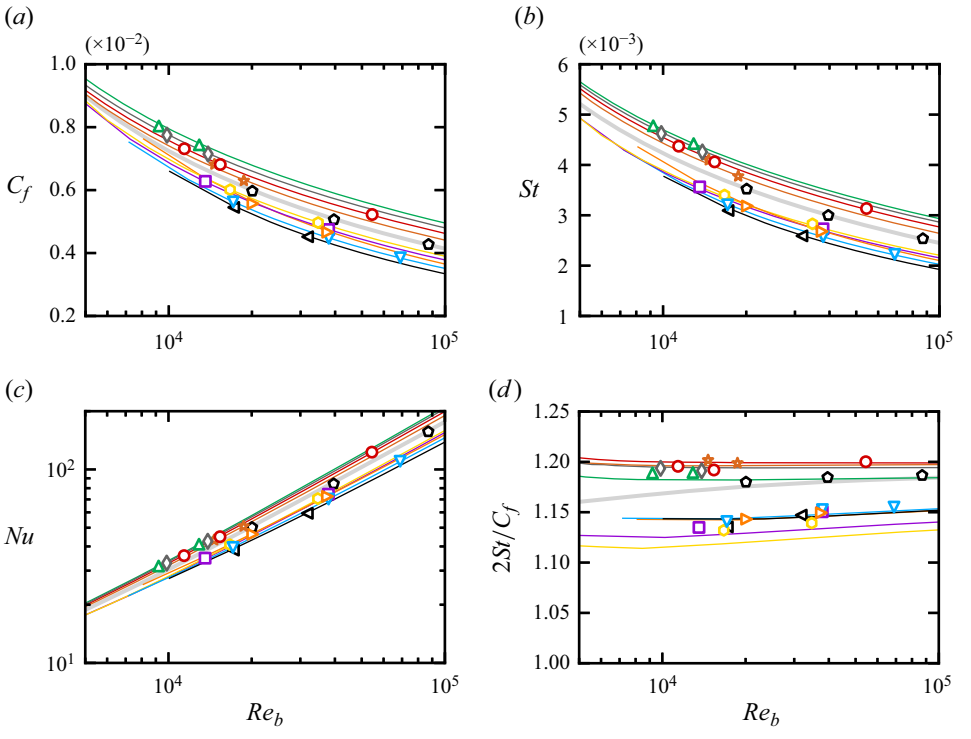

Figure 5. (*a*) Friction coefficient, (*b*) Stanton number, (*c*) Nusselt number and (*d*) Reynolds analogy factor as functions of the bulk Reynolds number $Re_b = 2h\rho_b u_b/\mu_m$. Solid lines indicate predictions obtained by inverting the variable-property transformations (4.1*a–c*), and symbols indicate DNS data for different mean-to-wall temperature ratios, with matching colours: $T_m/T_w = 0.4$ (black left triangles), $T_m/T_w = 0.5$, $T_w = 800$ K (orange downward triangles), $T_m/T_w = 0.5$, $T_w = 273.25$ K (blue right triangles), $T_m/T_w = 0.7$ (purple squares), $T_m/T_w = 0.8$ (gold hexagons), $T_m/T_w = 1.5$ (brown stars), $T_m/T_w = 2$ (red circles), $T_m/T_w = 2.5$ (grey diamonds), $T_m/T_w = 3$ (green upward triangles). Black pentagons refer to DNS data of passive scalars in plane channel flow with $Pr = 0.71$ from Pirozzoli *et al.* (2016).

(black pentagons) fall on top of the corresponding theoretical curves (light grey), we find significant deviations thereof in cases with property variations. In particular, we note that cases with a heated wall yield reduced friction and heat flux, whereas cases with a cooled wall yield an increase of momentum and heat transfer, with a scatter around the constant-property case of $\pm 25\,\%$ for both the friction coefficient and the Stanton number. We also report the heat transfer in terms of Nusselt number $Nu = Re_b\,St\,Pr$, although this representation tends to hide differences within a few per cent, thus the Stanton number should be preferred for accurate evaluation of theories. Theoretical predictions relying on use of the variable-property transformations (4.1*a–c*) are shown in the figure with solid lines of matching colours, and of course those are not universal as well. Notably, figure 5 shows that the resulting predictions match the DNS data to within 1–2 % accuracy for all cases, for both the friction and heat transfer coefficients, as shown quantitatively in figure 6. We further find that the analogy between momentum and heat transfer holds also in the case of variable-property flows, as the Reynolds analogy factor stays close to the constant property case, although this information alone is obviously not sufficient to recover the heat transfer and friction coefficients from the constant-property case. Note that the Reynolds analogy factor is not unity even in the constant-property case because $Pr = 0.72$.

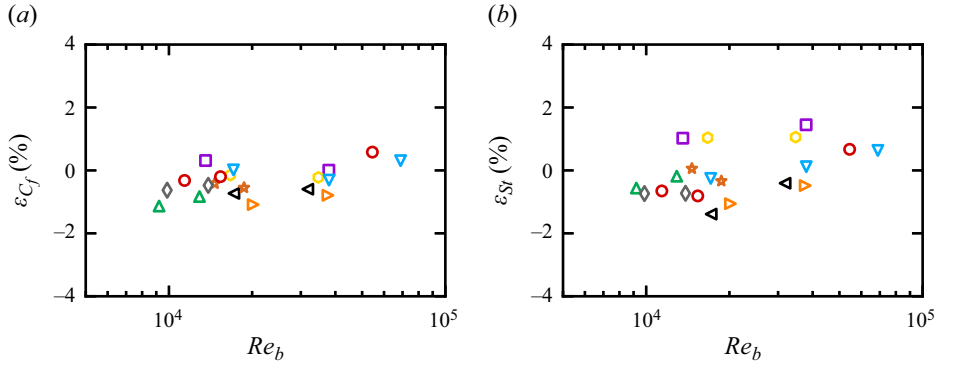

Figure 6. Percentage difference between DNS data and predicted (*a*) friction coefficient and (*b*) Stanton number as functions of the bulk Reynolds number $Re_b = 2h\rho_b u_b/\mu_m$. Symbols indicate DNS data for different mean-to-wall temperature ratios: $T_m/T_w = 0.4$ (left triangles), $T_m/T_w = 0.5$, $T_w = 800$ K (downward triangle), $T_m/T_w = 0.5$, $T_w = 273.25$ K (right triangles), $T_m/T_w = 0.7$ (squares), $T_m/T_w = 0.8$ (hexagons), $T_m/T_w = 1.5$ (stars), $T_m/T_w = 2$ (circles), $T_m/T_w = 2.5$ (grey diamonds), $T_m/T_w = 3$ (upward triangles).

6. Conclusions

Currently, predicting heat transfer through forced convection in real fluids depends heavily on fitting experimental data obtained decades ago, leading to uncertainties of up to 20–30 %. This significant variability is clearly reflected in the current DNS data. To address this uncertainty, we have developed a robust framework for estimating momentum and heat transfer coefficients. Our approach is grounded in the first principles of momentum and energy balance rather than empirical methods, offering the advantages of accuracy and generalizability. Similar to approaches used in high-speed turbulent boundary layers, our method relies on transformation kernels for velocity and temperature distributions.

Preliminary tests indicate that transformation kernels informed by DNS data can generate velocity and temperature distributions with excellent universality compared to the constant-property case. Evaluating momentum and heat transfer coefficients involves integrating the estimated velocity and temperature profiles obtained through the backward application of these transformation kernels, requiring an iterative procedure. Our results indicate that the method can accurately predict heat transfer and friction coefficients within 1–2 % compared to DNS data. Additionally, the developed method can determine mean temperature and velocity profiles alone, providing valuable information for establishing wall functions in simulations employing wall-modelled approaches.

We also acknowledge that cooling ducts in practical applications often feature rough walls rather than smooth ones (Chung *et al.* 2021; De Maio *et al.* 2023; Zhong, Hutchins & Chung 2023). This raises questions about the applicability of the current transformations to complex surface patterns. In such cases, the effects of density and viscosity variations lead to a much more intricate flow physics compared to constant-property flows. Several mechanisms and parameters remain to be studied, including the precise mechanisms responsible for friction and heat transfer variation, the impact on turbulence length scales, the dependency of Prandtl number and heat capacity on the temperature, and the influence of the working fluid. We plan to investigate these aspects in future studies.

We believe that the proposed approach could have important implications in closely related fields, as mixed and natural convection. In principle, we see no reason why the

same approach should not be applicable to these flow problems, as the transformations are rooted in the mean momentum and thermal balance, which are universal.

Acknowledgements. We acknowledge CHRONOS for awarding us access to Piz Daint, at the Swiss National Supercomputing Centre (CSCS), Switzerland. We also acknowledge EuroHPC for access to LEONARDO based at CINECA, Casalecchio di Reno, Italy.

Declaration of interests. The authors report no conflict of interest.

Data availability. The DNS data are available at http://newton.dma.uniroma1.it. Model coefficients can be generated at http://www.thermoturb.com.

Author ORCIDs.
Davide Modesti https://orcid.org/0000-0003-2214-5799;
Sergio Pirozzoli https://orcid.org/0000-0002-7160-3023.

Appendix A

We solve the fully compressible Navier–Stokes equations for a perfect heat-conducting gas,

$$\frac{\partial \rho}{\partial t} + \frac{\partial \rho u_i}{\partial x_i} = 0, \tag{A1a}$$

$$\frac{\partial \rho u_i}{\partial t} + \frac{\partial \rho u_i u_j}{\partial x_j} = -\frac{\partial p}{\partial x_i} + \frac{\partial \sigma_{ij}}{\partial x_j} + f\delta_{i1}, \tag{A1b}$$

$$\frac{\partial \rho s}{\partial t} + \frac{\partial \rho u_j s}{\partial x_j} = \frac{1}{T}\left(-\frac{\partial q_j}{\partial x_j} + \sigma_{ij}\frac{\partial u_i}{\partial x_j}\right) + Q, \tag{A1c}$$

where u_i, $i = 1, 2, 3$, is the velocity component in the ith direction, ρ is the density, p is the pressure, $s = c_v \log(p\rho^{-\gamma})$ is the entropy per unit mass, and $\gamma = c_p/c_v = 1.4$ is the specific heat ratio. The components of the heat flux vector q_j and of the viscous stress tensor σ_{ij} are

$$\sigma_{ij} = \mu\left(\frac{\partial u_i}{\partial x_j} + \frac{\partial u_j}{\partial x_i} - \frac{2}{3}\frac{\partial u_k}{\partial x_k}\delta_{ij}\right), \tag{A2}$$

$$q_j = -k\frac{\partial T}{\partial x_j}, \tag{A3}$$

where the dependence of the viscosity coefficient on temperature is accounted for through Sutherland's law, and $k = c_p\mu/Pr$ is the thermal conductivity, with $Pr = 0.72$. Use of the entropy equation to replace the energy equations is here dictated from the possibility to relax the acoustic time step limitation with semi-implicit time stepping Modesti & Pirozzoli (2018), thus yielding a computational efficiency comparable to a variable-property incompressible solver.

The forcing term f in (A1b) is evaluated at each time step in order to discretely enforce constant mass flow rate in time. Similarly, a uniform bulk heating/cooling term is added to the entropy equation to make the mixed mean temperature exactly constant in time. Since we solve for the entropy equation, this is achieved by correcting the local temperature at

each grid point and each Runge–Kutta sub-step as follows:

$$T(x, y, z, t) \rightarrow T(x, y, z, t) - T_m(t) + T_m^*, \tag{A4}$$

where $T_m(t)$ is the mixed mean temperature before the correction, and T_m^* is the target value. The updated temperature value is then used to re-evaluate the entropy at the current time.

References

ABE, H. & ANTONIA, R.A. 2017 Relationship between the heat transfer law and the scalar dissipation function in a turbulent channel flow. *J. Fluid Mech.* **830**, 300–325.

ALCÁNTARA-ÁVILA, F., HOYAS, S. & PÉREZ-QUILES, M.J. 2021 Direct numerical simulation of thermal channel flow for $Re_\tau = 5000$ and $Pr = 0.71$. *J. Fluid Mech.* **916**, A29.

BERNARDINI, M., MODESTI, D., SALVADORE, F. & PIROZZOLI, S. 2021 STREAmS: a high-fidelity accelerated solver for direct numerical simulation of compressible turbulent flows. *Comput. Phys. Commun.* **263**, 107906.

BERNARDINI, M., MODESTI, D., SALVADORE, F., SATHYANARAYANA, S., POSTA, G.D. & PIROZZOLI, S. 2023 STREAmS-2.0: supersonic turbulent accelerated Navier–Stokes solver version 2.0. *Comput. Phys. Commun.* **285**, 108644.

CEBECI, T. & BRADSHAW, P. 1984 *Physical and Computational Aspects of Convective Heat Transfer*. Springer Science & Business Media.

CHUNG, D., HUTCHINS, N., SCHULTZ, M.P. & FLACK, K.A. 2021 Predicting the drag of rough surfaces. *Annu. Rev. Fluid Mech.* **53**, 439–471.

CLAUSER, F.H. & FRANCIS, H. 1956 The turbulent boundary layer. *Adv. Appl. Mech.* **4**, 1–51.

DE MAIO, M., LATINI, B., NASUTI, F. & PIROZZOLI, S. 2023 Direct numerical simulation of turbulent flow in pipes with realistic large roughness at the wall. *J. Fluid Mech.* **974**, A40.

DITTUS, F.W. & BOELTER, L.M.K. 1985 Heat transfer in automobile radiators of the tubular type. *Intl Commun. Heat Mass Transfer* **12** (1), 3–22.

VAN DRIEST, E.R. 1951 Turbulent boundary layer in compressible fluids. *J. Aero. Sci.* **18**, 145–160.

GNIELINSKI, V. 1976 New equations for heat and mass transfer in turbulent pipe and channel flow. *Intl Chem. Engng* **16**, 359–367.

GRAY, D. & GIORGINI, A. 1976 The validity of the Boussinesq approximation for liquids and gases. *Intl J. Heat Mass Transfer* **19** (5), 545–551.

GROSSMANN, S. & LOHSE, D. 2000 Scaling in thermal convection: a unifying theory. *J. Fluid Mech.* **407**, 27–56.

HASAN, A.M., LARSSON, J., PIROZZOLI, S. & PECNIK, R. 2023 Incorporating intrinsic compressibility effects in velocity transformations for wall-bounded turbulent flows. *Phys. Rev. Fluids* **8** (11), L112601.

HASAN, A.M., LARSSON, J., PIROZZOLI, S. & PECNIK, R. 2024 Estimating mean profiles and fluxes in high-speed turbulent boundary layers using inner/outer-layer scalings. *AIAA J.* **62** (2), 848–853.

INCROPERA, F.P., DEWITT, D.P., BERGMAN, T.L., LAVINE, A.S. 1996 *Fundamentals of Heat and Mass Transfer*. Wiley.

KADER, B.A. 1981 Temperature and concentration profiles in fully turbulent boundary layers. *Intl J. Heat Mass Transfer* **24** (9), 1541–1544.

KAKAC, S., LIU, H. & PRAMUANJAROENKIJ, A. 2002 *Heat Exchangers: Selection, Rating, and Thermal Design*. CRC Press.

KALLER, T., PASQUARIELLO, V., HICKEL, S. & ADAMS, N.A. 2019 Turbulent flow through a high aspect ratio cooling duct with asymmetric wall heating. *J. Fluid Mech.* **860**, 258–299.

KIM, Y., GUEZENNEC, D., STRETCH, J. 1990 The structure of turbulent channel flow with passive scalar transport. In *Proceedings of the Summer Program, Centre for Turbulence Research, Stanford University*, pp. 127–138.

KUMAR, V. & LARSSON, J. 2022 Modular method for estimation of velocity and temperature profiles in high-speed boundary layers. *AIAA J.* **60** (9), 5165–5172.

LEE, J., JUNG, S.Y., SUNG, H.J. & ZAKI, T.A. 2013 Effect of wall heating on turbulent boundary layers with temperature-dependent viscosity. *J. Fluid Mech.* **726**, 196–225.

LEE, J., JUNG, S.Y., SUNG, H.J. & ZAKI, T.A. 2014 Turbulent thermal boundary layers with temperature-dependent viscosity. *Intl J. Heat Fluid Flow* **49**, 43–52.

MODESTI, D. & PIROZZOLI, S. 2016 Reynolds and Mach number effects in compressible turbulent channel flow. *Intl J. Heat Fluid Flow* **59**, 33–49.

MODESTI, D. & PIROZZOLI, S. 2018 An efficient semi-implicit solver for direct numerical simulation of compressible flows at all speeds. *J. Sci. Comput.* **75** (1), 308–331.
MUSKER, A.J. 1979 Explicit expression for the smooth wall velocity distribution in a turbulent boundary layer. *AIAA J.* **17** (6), 655–657.
NAGIB, H.M. & CHAUHAN, K.A. 2008 Variations of von Kármán coefficient in canonical flows. *Phys. Fluids* **20** (10), 101518.
NIKURADSE, J. 1933 Stromungsgesetze in rauhen Rohren. *Vdi-Forschungsheft* **361**, 1.
PATEL, A., BOERSMA, B.J. & PECNIK, R. 2016 The influence of near-wall density and viscosity gradients on turbulence in channel flows. *J. Fluid Mech.* **809**, 793–820.
PATEL, A., BOERSMA, B.J. & PECNIK, R. 2017 Scalar statistics in variable property turbulent channel flows. *Phys. Rev. Fluids* **2** (8), 084604.
PETUKHOV, B.S. 1970 Heat transfer and friction in turbulent pipe flow with variable physical properties. *Adv. Heat Transfer* **6**, 503–564.
PINELLI, A., UHLMANN, M., SEKIMOTO, A. & KAWAHARA, G. 2010 Reynolds number dependence of mean flow structure in square duct turbulence. *J. Fluid Mech.* **644**, 107–122.
PIROZZOLI, S. 2023 An explicit representation for mean profiles and fluxes in forced passive scalar convection. *J. Fluid Mech.* **968**, R1.
PIROZZOLI, S., BERNARDINI, M. & ORLANDI, P. 2016 Passive scalars in turbulent channel flow at high Reynolds number. *J. Fluid Mech.* **788**, 614–639.
PIROZZOLI, S. & MODESTI, D. 2023 Direct numerical simulation of one-sided forced thermal convection in plane channels. *J. Fluid Mech.* **957**, A31.
PIROZZOLI, S. & MODESTI, D. 2024 Mean temperature and concentration profiles in turbulent internal flows. *Intl J. Heat Fluid Flow* **109**, 109544.
PIROZZOLI, S., ROMERO, J., FATICA, M., VERZICCO, R. & ORLANDI, P. 2021 One-point statistics for turbulent pipe flow up to $Re_\tau \approx 6000$. *J. Fluid Mech.* **926**, A28.
SIEDER, E.N. & TATE, G.E. 1936 Heat transfer and pressure drop of liquids in tubes. *Ind. Engng Chem.* **28** (12), 1429–1435.
SLEICHER, C.A. & ROUSE, M.W. 1975 A convenient correlation for heat transfer to constant and variable property fluids in turbulent pipe flow. *Intl J. Heat Mass Transfer* **18** (5), 677–683.
SPARROW, E.M., LLOYD, J.R. & HIXON, C.W. 1966 Experiments on turbulent heat transfer in an asymmetrically heated rectangular duct. *J. Heat Transfer* **88**, 170–174.
TRETTEL, A. & LARSSON, J. 2016 Mean velocity scaling for compressible wall turbulence with heat transfer. *Phys. Fluids* **28** (2), 026102.
VOLPIANI, P.S, IYER, P.S., PIROZZOLI, S. & LARSSON, J. 2020 Data-driven compressibility transformation for turbulent wall layers. *Phys. Rev. Fluids* **5** (5), 052602.
WHITE, F.M. 1974 *Viscous Fluid Flow*. McGraw-Hill.
XIA, Y., ROWIN, W.A., JELLY, T., MARUSIC, I. & HUTCHINS, N. 2022 Investigation of cold-wire spatial and temporal resolution issues in thermal turbulent boundary layers. *Intl J. Heat Fluid Flow* **94**, 108926.
YEH, F.C. & STEPKA, F.S. 1984 Review and status of heat-transfer technology for internal passages of air-cooled turbine blades. *NASA Tech. Rep.* 2232. NASA.
YERRAGOLAM, G.S., HOWLAND, C.J., STEVENS, R.J.A.M., VERZICCO, R., SHISHKINA, O. & LOHSE, D. 2024 Scaling relations for heat and momentum transport in sheared Rayleigh–Bénard convection. arXiv:2403.04418
ZHONG, K., HUTCHINS, N. & CHUNG, D. 2023 Heat-transfer scaling at moderate Prandtl numbers in the fully rough regime. *J. Fluid Mech.* **959**, A8.
ZONTA, F. 2013 Nusselt number and friction factor in thermally stratified turbulent channel flow under non-Oberbeck–Boussinesq conditions. *Intl J. Heat Fluid Flow* **44**, 489–494.
ZONTA, F., MARCHIOLI, C. & SOLDATI, A. 2012 Modulation of turbulence in forced convection by temperature-dependent viscosity. *J. Fluid Mech.* **697**, 150–174.